EXPERIMENTAL INVESTIGATION AND NUMERICAL SIMULATION OF SHEAR BEHAVIOUR OF RC T-BEAM SPECIMENS WITH OR WITHOUT SFRP-STRIPS UNDER CYCLIC LOADING

George C. Manos[1], Konstantinos B. Katakalos[1] and Marios Theofanous[2]

[1,2] Aristotle University of Thessaloniki
School of Engineering, Egnatia street, University Campus, Thessaloniki, Greece
e-mail: kkatakal@auth.gr, gcmanos@civil.auth.gr

[2] University of Birmingham
School of Engineering, Edgbaston, Birmingham, UK, B15 2TT
m.theofanous@bham.ac.uk

Keywords: Shear strengthening, Reinforced concrete T-beams, FRPs, Experimental investigation, Numerical simulation FRP strip anchoring instructions.

Abstract. *The successful validation of a numerical model is presented that can realistically approximate the shear behavior of reinforced concrete (RC) T-section beams strengthened against shear with externally applied open hoop steel fiber reinforcing polymer (SFRP) strips. For this purpose, the measured load-deformation response of three (3) full-scale R/C beam specimens is utilized. These specimens were imposed in a cyclic loading sequence up to failure. Open hoop steel FRP strip shear reinforcement was applied externally to upgrade the shear capacity of two (2) RC beam specimens. For the first specimen the SFRP strips were applied without anchorage, whereas for the other strengthened specimen the SFRP strips were attached together with a novel anchoring device. The successful numerical simulation predicts with a very good degree of approximation the observed load-deformation behavior and the ultimate shear capacity of all these specimens as well as the observed modes of failure including diagonal concrete cracking, debonding of the CFRP strips in the case of no anchoring, or the plastification of parts of the anchoring devices plus the adjacent crushing of the concrete.*

1   INTRODUCTION

Reinforced Concrete (R/C) structures represent a substantial portion of the current infrastructure and building stock in most countries worldwide. A large percentage of these were built several decades ago and in some cases require retrofitting or structural upgrading in order to conform to more stringent design regulations, to accommodate additional live loads due to possible changes in the building's function or to make up for the loss of strength brought about by environmental parameters that speed up structural deterioration. Moreover, the rapid evolution of seismic codes over the past two decades, which utilizes the knowledge gained following devastating earthquakes, necessitates the structural upgrading of most concrete structures that were built according to older design regulations, following a different design philosophy, in which the role of ductility was not central to the design process. On the contrary, all current seismic design codes pay particular attention to enforce ductile behavior on the various R/C structural elements, which is accomplished by prohibiting shear types of failure and favoring instead flexural types of failure with sufficient ductility [1-4, 10-18]. This ductile behavior is also desirable when one is faced with the task of designing a retrofitting scheme that aims at upgrading the seismic performance of R/C structures designed by older design codes [19]. This paper deals with the objective of upgrading the shear capacity of R/C T-beams, that are poorly reinforced against shear, as part of such a retrofitting scheme [5,17,18,20].

Among several upgrading techniques available, the utilization of FRP sheets or plates that can be attached externally to existing structural components with the aid of resin has attracted considerable attention from both academics and practicing engineers [2,6,15,28]. Various researchers have derived models for the prediction of the bond-slip response and required anchor lengths of FRP sheets attached to concrete [22,24-26,29]. Depending on the application, fibre reinforcing polymer (FRP) sheets can be employed to increase the flexural strength, the shear strength, the ductility and the serviceability performance of R/C structures, utilizing these FRP sheets as additional external reinforcement.

FRP sheets possess very high strength in the orientation of their fibres; however only a small part of the available strength can be exploited in practice, due to the onset of debonding at relatively small strains, which can initiate either at the ends of the FRP sheets, due to insufficient anchoring or within the mid-parts of the FRP sheets, when anchoring is provided at the FRP-strip ends, following the formation of cracks in the concrete [5-12,27]. Therefore, the development of innovative means for effective anchorage of the FRP sheets/plates in the concrete volume, which ensures the satisfactory transfer of forces from the FRP sheet to the concrete part of the structural member and allows for a more efficient utilization of the FRP strength, is warranted [24–28].

In the present paper, a novel anchorage device [13] for FRP sheets employed as external shear reinforcement, which was recently developed at the Laboratory of Strength of Materials and Structures of Aristotle University of Thessaloniki is studied numerically. Its effectiveness has been experimentally verified. [18,25,26] The aim of the present study is to replicate numerically the experimentally obtained results and to identify the key parameters controlling the structural response of reinforced concrete T-beams strengthened against shear by external FRP reinforcement, that will allow the optimization of the anchorage device and hence the more effective utilization of the FRP sheets, thus leading to more efficient design. Finally the R/C concrete T-beams are imposed to a cyclic loading sequence.

2   EXPERIMENTAL SETUP

Several theoretical and experimental studies [4,9,15] have been carried out to analyze the phenomenon of the shear failure of reinforced concrete (RC) beams. Russo et al. [22] presents a comprehensive review of various proposed methods for predicting the shear behavior of reinforced concrete beams without any transverse reinforcement. In the design of R/C beams, this is usually considered as an initial condition that is supplemented by the strength provided by the transverse reinforcement in order to predict the total shear capacity of such a structural element. Following this rationale a comprehensive experimental program has been designed and carried out at the Laboratory of Experimental Structural Mechanics at the Aristotle University of Thessaloniki aimed to assess the structural efficiency and effectiveness of shear strength provided to R/C beams by externally attached open hoop FRP transverse shear reinforcement. Initially, one R/C T-beam specimens with only longitudinal reinforcement was tested. Two identical R/C T-beam specimens were then tested which were provided with open hoop FRP strips external shear reinforcement in order to study in this way the additional shear strength that can be attained by such a strengthening scheme. This open hoop FRP strip shear reinforcement was examined in two distinct forms. First, these open hoop FRP strips were simply attached on the external surface of the R/C specimens. The prevailing mode of failure for this specimen is the debonding of the FRP strips, which renders this type of shear reinforcement ineffective. This is because the FRP strips' debonding occurs long before the tensile strength capacity of such FRP strips is reached. In order to prohibit such a premature debonding type of failure a novel anchorage device [24–27] is introduced together with the open hoop FRP strips that can be attached relatively easily at R/C T-beams, which is the primary practical application. The second T-beams was strengthened utilizing this technique.

2.1   T-section beam tests

Three cantilever reinforced concrete beams with a T-section were fabricated and tested under cycling loading conditions at the Laboratory of Strength of Materials and Structures of Aristotle University of Thessaloniki. The reinforcing details are depicted in figure 1. The set-up consists of a T-beam with dimensions 120 by 360 mm with a slab width of 360mm and a rectangular column with cross sectional dimensions 400 by 500 mm. The part of the specimen that resembles the column was securely fastened to a rigid wall using two steel I-beams. The free end of the beam was attached via a hinge to a 2500 kN capacity hydraulic actuator which was used to apply the cycling load. The load was controlled with a 1000 kN capacity load cell under deflection control, driven by a personal computer. After applying three cycles in elastic region, loading cycles were increased gradually up to failure. Same loading methodology was applied to all specimens. The beam's free end deflection and moment curvature at the maximum moment region were measured using LVDT's. LVDT's were also positioned vertical to the longitudinal axis of the beam to ensure that the beam did not deflect out of plain. LVDT's were also placed at an angle of 45°. SFRP strains were measured with strain gauges. Strain gauges were attached on 8 consecutive SFRP tapes starting from the second from the fixed end. A strain gauge was attached to the mid-height of each SFRP tape along the fiber direction. Finally the time history of the loading sequence is presented in figure 2.
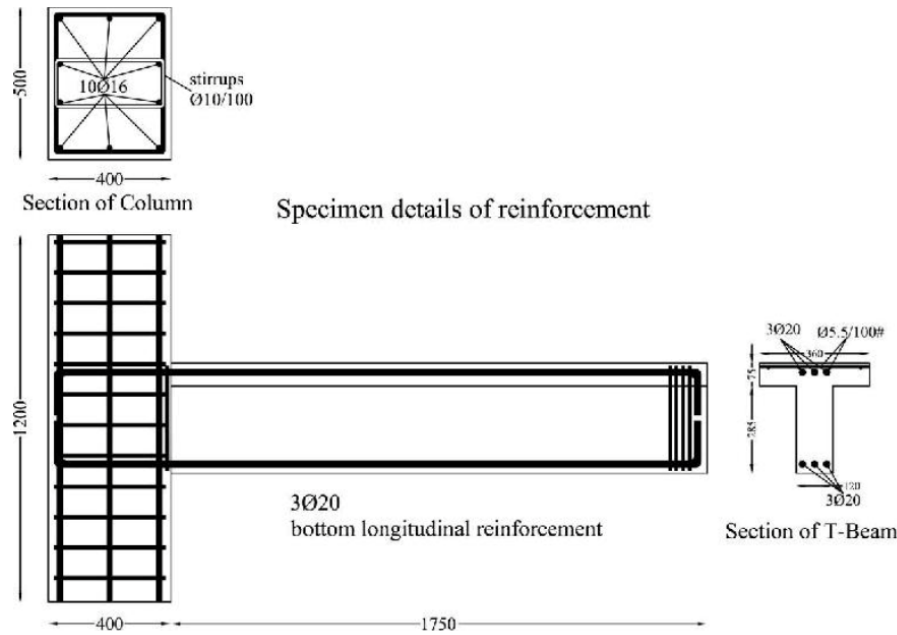
Figure 1. Specimen Details and Reinforcement

Initially, one concrete T-beam specimen both without any SFRP, namely CTB was tested to obtain the basic structural response. This test was utilized in the present numerical study to calibrate the material parameters of the concrete material model. Subsequently, two more specimens without any steel stirrups were reinforced against shear by externally attaching U-shape open-hoop SFRP strips with and without an anchorage scheme. (named TB150 and TB150a) The spacing of SFRP strips was considered equal to 150 mm. The anchorage was provided by the novel anchorage device [24] depicted in some detail in figures 3a and 3b. In this anchoring device a steel rod is used to wrap around it the FRP strip; this steel rod is secured by a steel plate of equal length which is bolted by two anchor bolts as shown in figure 3b.
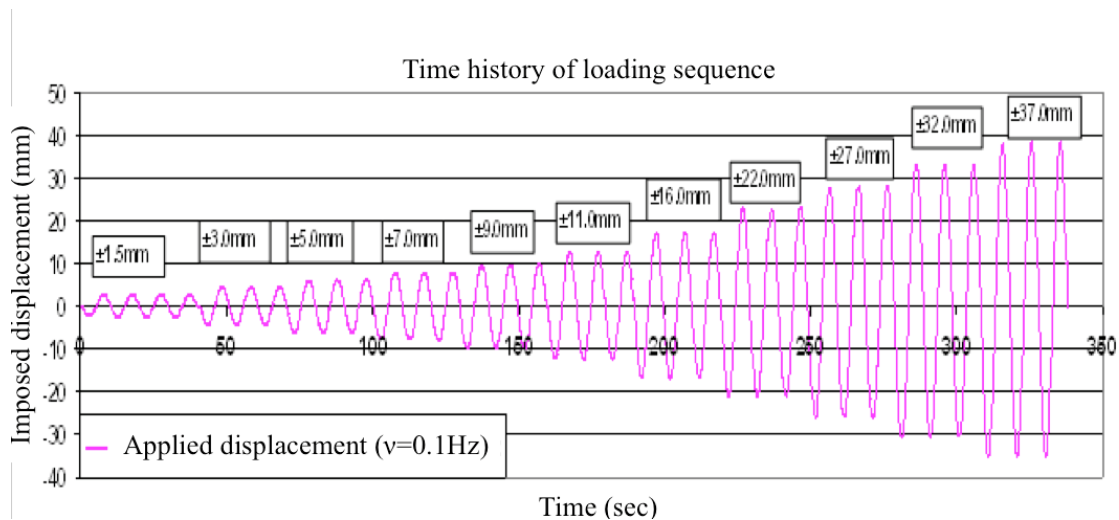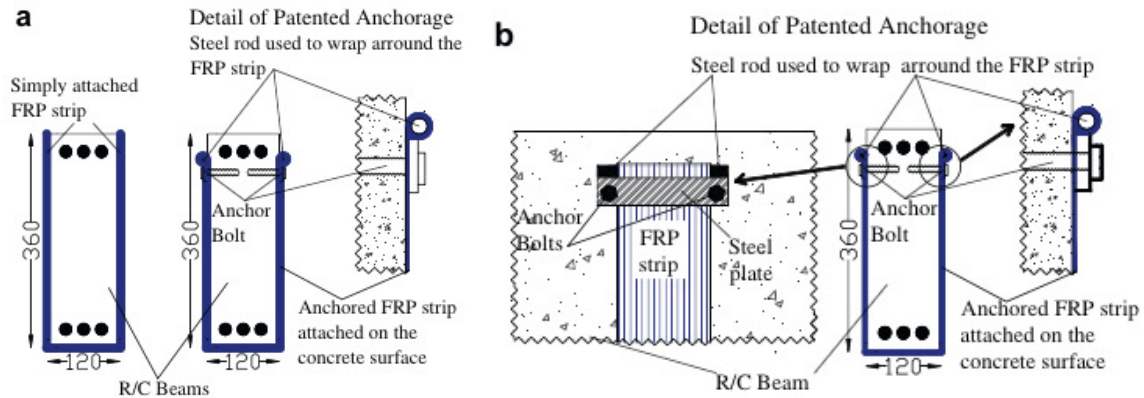

Figure 2. Time history of loading sequence

Figures 3a and 3b. Cross section of the tested specimens
with the reinforcement details and the proposed anchoring device (dimensions in mm).

Table 1 lists all the particular aspects that characterize each one of these three specimens.

Table1. Summary of beam tests.

Designation	Shear rein-force-ment	Mean concrete cylindrical strength (Mpa)	Width of SFRP strip (mm)	Spacing of SFRP strip (mm)	Anchora ge	Measured ultimate shear capacity $^{exp}V_{max}$ (kN)	Mode of failure
CTB	No				N/A	37.25	Diagonal crack
TB150	SFRP (1layer)	22.40	100	150	No	73.20	Debonding
TB150a	SFRP (1layer)				Yes	182.40	Anchorage failure

2.2 Material tests

A series of standard tests have been carried out in order to establish the basic material properties for these beam specimens; e.g. basic material properties for the concrete, the reinforcing bars, the SFRP strips as well as the steel plates and steel bolts employed in the anchoring device. These experimentally derived material properties were utilized in the subsequent numerical study. The measured mean concrete cylindrical strength for each specimen is listed in column 3 of Table 1 and is equal to 22.4Mpa. The longitudinal and transverse reinforcement were grade S500, whilst the steel plates were grade S235. The bolts utilized in the anchoring device were manufactured by HILTI and are designated as HILTI HUS herein. The full stress-strain response of all steel parts was experimentally determined and utilized in the numerical studies. The experimentally determined Young's modulus E, yield strength f_y and ultimate strength f_u are reported in Table 2.

Finally, unidirectional tension tests were conducted on resin rich SFRP sheets up to failure to obtain the Young's modulus (E_1) and strength (fu_1) in their fibre orientation and the Poisson's ratio ($v_{12} = (E1/E2)v_{21}$). The remaining two material properties pertaining to the orthotropic nature of the material under the plane stress assumption, namely the transverse Young's

modulus E_2 and the shear modulus G_{12}, were derived by applying the conventional rule of mixture for composites [17], taking into account the manufacturer's specifications for the resin and the FRP sheets (see acknowledgements) and the experimentally determined volume fraction of resin and FRP sheets.

Both the experimentally and the analytically determined material properties are reported in Table 3. It should be noted that the analytical values obtained by applying the rule of mixture for E_1 and v_{12} compare very well (discrepancy within 5%) with the experimental ones.

Table 2. Material properties of employed steel plates, rebars and bolts.

Material property	Longitudinal rebars of d = 20 mm diameter	Steel plates of anchoring device	Anchor bolts Hilti HUS
E (MPa)	202,700	210,000	210,000
f_y (MPa)	527	255	800
f_u (MPa)	645	390	917

Table 3. Material properties of SFRP.

Material property	E_1 (Mpa)	V_{12}	F_{u1} (Mpa)	E_2 (Mpa)	G_{12} (Mpa)
SFRP	36,350	0.312	330	4,400	1,900

2.3 Summary of observed behavior – modes of failure

The key findings of all beam tests are summarized in Table 1, where the ultimate shear force ($^{exp}V_{max}$) resisted by these specimens is listed in column 7 of this table. As can be seen, the shear strength of the control rectangular beam (CTB) without any stirrups SFRP strips was recorded equal to 37.25 kN. From the results shown in Table 1, it is evident that the maximum recorded shear capacity for the two strengthened T-beams with SFRP strips was significantly greater than the shear capacity of CTB specimen. The observed mode of failure is listed in column 8 of Table 1. As can be seen, when SFRP strips are without anchors the debonding mode of failure of the FRP strips prevails. This debonding mode of failure limits the observed shear capacity increase to 96.5% (nearly 2 times larger than the initial value of 37.25 kN), when the shear capacity of the strengthened specimen is compared to that of specimen CTB (without any shear reinforcement). When the novel anchoring device was utilized for prohibiting this debonding mode of failure it resulted in shear capacity increase of up to 390% (4.9 times larger than the initial value of 37.25 kN). It should be noted that CTB has no internal shear reinforcement. The beneficial effect of anchoring the U-shape open-hoop SFRP strips in order to inhibit the debonding mode of failure is thus demonstrated. The subsequent numerical study will focus on these important features of the observed behavior, that is the prevailing mode of failure and the measured ultimate shear capacity ($^{exp}V_{max}$).

3 NUMERICAL ANALYSIS

The general purpose FE software ABAQUS [9] was employed to generate FE models to simulate numerically the structural response of the previously described concrete beams strengthened with externally attached FRP sheets. The generated models were validated against all respective experimental results. The aim of this part of the study is to generate reliable FE models that can be utilized to enhance the understanding of the fundamental struc-

tural response of the FRP shear strengthening scheme of R/C T-beams with and without anchorage devices, under cyclic loadings and hence optimize the anchorage device design.

3.1 Modeling assumptions

The mean measured specimen geometries were utilized to simulate the test specimens. The full 3D geometry of the concrete volume and the steel plates employed for the anchorage of the SFRP was modeled with 3-D brick-type F.E. elements, whilst the FRP sheets were idealized as planar F.E. elements and their actual thickness (0.75 mm) was utilized as a section property. The bolts were assumed cylindrical with a diameter equal to the equivalent diameter corresponding to the net bolt area (i.e. the threaded part of the bolts was not explicitly modeled). A further idealization pertinent to the bolt assembly simulation is the assumption that the bolt-hole diameter of the steel plate is equal to the assumed bolt diameter (i.e. the clearance has not been accounted for).

In order to reduce the computational cost, the symmetry of the structure with respect to the x–y mid-plane was exploited, by numerically simulating one quarter of the physical model and applying the appropriate boundary conditions at each of the two planes of symmetry as shown in figure 4. The load was applied incrementally as prescribed displacement on a steel plate (SP1) at the point of load application, which was applied iteratively utilizing a smooth amplitude curve available in ABAQUS. Restraint of the structure in the direction of the prescribed displacement was provided by fixing all degrees of freedom of nodes at the supporting element. The sum of the reaction forces in all nodes of the supporting element yields the total reaction that is exerted to the model structure and will be compared with $^{exp}V_{max}$ of Table 1.
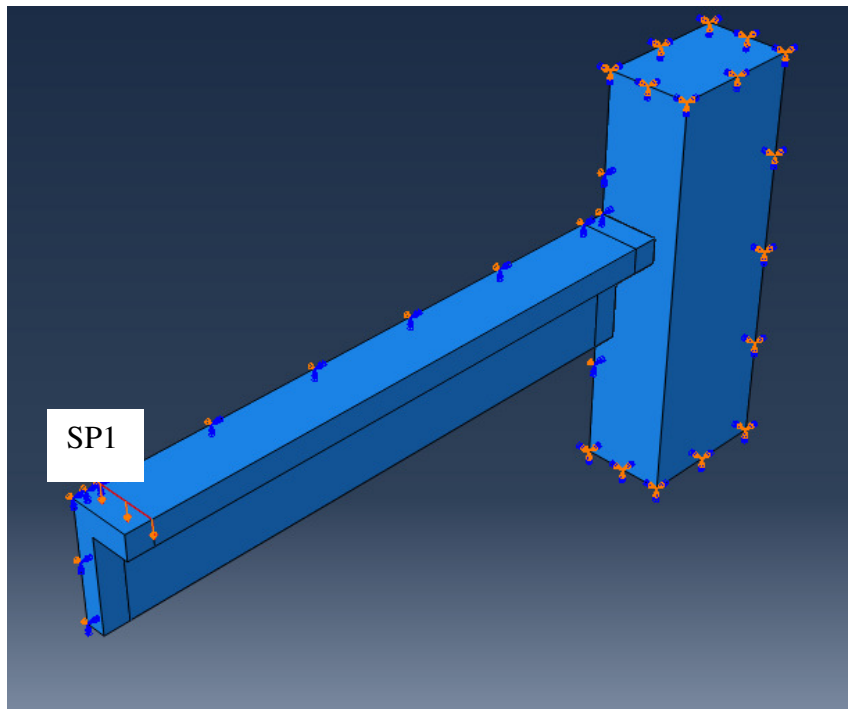

Figure 4. Modeled geometry and applied boundary conditions.

The contact between the various parts of the model (steel bolts, steel plates and concrete volume) was explicitly modeled and a friction coefficient equal to 0.3 was assumed for tangential contact behavior. Variation of the friction coefficient applied to the bolt-concrete inter-

face between the idealized frictionless and rough contact extreme cases was attempted, but no significant effect on the overall solution was observed. Moreover, in order to reduce computational cost, the actual detail of the cylindrical rod of the anchoring device through which load is transferred from the FRP strips to the concrete beam through the steel plate was somewhat simplified (see figures 3b and 5); towards this end, the displacements of the SFRP's edge were constrained to be equal to the respective displacements of the steel plate's mid plane for the numerical representation of the anchoring device. The interface between the SFRP strip and the concrete was simulated as a cohesive zone endowed with a suitable traction separation response, the properties of which are discussed below.
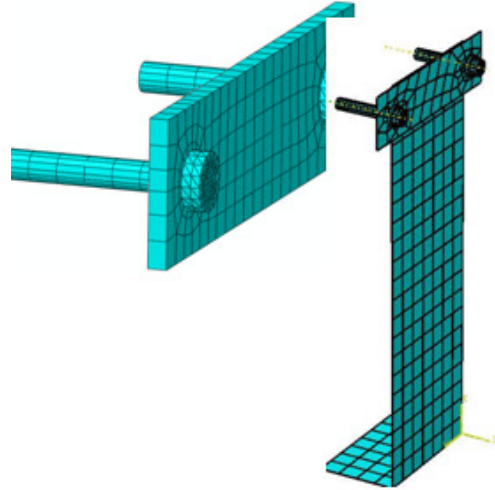

Figure 5. Finite element discretization of the anchoring device

3.2   Material modeling

The auxiliary test results reported previously were utilized herein to define the material response. The SFRP sheets were assumed orthotropic under plane stress conditions and the material properties reported in Table 3 were adopted. The tensile failure in the principal direction was considered and the ultimate stress reported in Table 3 was adopted, whilst other failure modes were considered irrelevant to the present study. A fracture energy equal to 0.01 was assumed to simulate damage evolution, which was rapid, due to the severe stress concentration following the onset of failure. Steel plates, longitudinal reinforcing bars, steel stirrups and steel bolts and plates were assumed elastic-isotropic hardening and the experimentally obtained stress–strain curves for the steel used for these parts were converted into the true stress-logarithmic plastic strain format according to Eqs. (1) and (2) and utilized to define the material response.

$$\sigma_{true} = \sigma_{nom}(1 + \varepsilon_{nom}) \quad \text{eq.1,} \qquad \varepsilon_{ln}^{pl} = \ln(1 + \varepsilon_{nom}) - \frac{\sigma_{true}}{E} \quad \text{eq.2}$$

The damaged plasticity model for concrete available in the ABAQUS material library was adopted to model concrete response, since it has been shown to perform satisfactorily in similar applications [23]. All material parameters were initially calibrated to accurately simulate the response of the control T-beam specimen CTB. The values adopted for the relevant material parameters, namely the angle of dilation h, the eccentricity, the ratio of equibiaxial to uni-

axial compressive stress fb0/fc0, the ratio of the second stress invariant on the tensile meridian to that on the compressive meridian at initial yield Kc and the viscosity parameter were 40, 0.1, 1.16, 0.666 and 0 respectively and were all within the range encountered in literature [23]. In accordance with similar studies [18], the stress strain response of concrete in compression was derived according to Saenz [23], whilst the tension stiffening response was defined in terms of tensile stress and axial deformation according to Cornelissen et al. [12], assuming a fracture energy equal to 0.06. The Young's modulus E and tensile strength f_{ct} were determined according to ACI [1] as a function of the compressive cylindrical strength, whilst Poisson's ratio was assumed equal to 0.2. The comparison between this assumed in the numerical simulation stress–strain concrete behavior and the one measured by testing concrete cylindrical specimens taken during the construction of the beam specimens is depicted in figure 6. It must be borne in mind that these specimens were simply loaded in compression in such a way that the descending branch of the stress–strain curve could not be obtained.
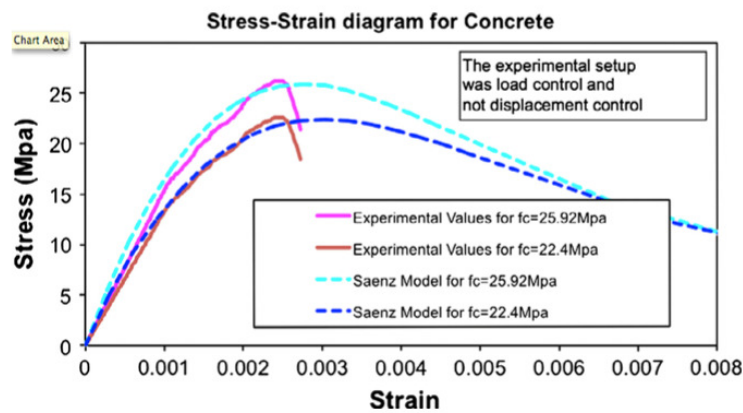

Figure 6. Measured and assumed concrete stress-strain behavior
in unconfined uniaxial compression.

The resin rich layer, within which the debonding of the FRP strip from the concrete volume occurs, was modeled as a cohesive zone [3] endowed with a traction-separation response. The initial elastic stiffness for all three modes of debonding was set equal to 106 N/ mm2, which is within the range of values proposed by Turon et al. [28]. The quadratic stress-based damage initiation criterion available in ABAQUS was adopted, with the stress limit in all three principal directions being equal to the respective tensile concrete strength. Damage evolution was defined in terms of fracture energy with linear softening, whilst mixed mode behavior was accounted for according to the model proposed by Benzeggagh and Kenane [8], with a power coefficient equal to 1.45, in accordance with the proposals of Obaidat et al. [29]. Best results were obtained for a fracture energy in both shearing and peeling modes equal to 0.25 (GII = GIII = 0.25 N/mm2), whilst the fracture energy GI associated with the opening mode was set equal to 0.025. It should be noted that overall response is relatively insensitive to the assumed elastic stiffness and limiting stress adopted, but these properties have a significant effect on the numerical cohesive zone length [16,28], which defines the minimum required mesh size.

3.3 Non-linear analysis and discretization

Linear 8-noded brick elements were adopted for the discretization of the concrete beam, steel bolts, steel plates and loading plates, whilst the longitudinal reinforcing bars and the steel stirrups were discretized with linear truss elements embedded in the concrete region (i.e.

no relative displacement between reinforcement and concrete was allowed for). Linear 4-noded shell elements were used to discretize the SFRP sheets, the degrees of freedom (DOF) of which were tied to the respective DOFs of the underlying 8-noded 3D cohesive elements. The mesh size was dictated by the attempt to minimize computational time whilst maintaining accuracy and, upon extensive mesh convergence studies, a uniform mesh size of 15 mm was adopted for the concrete beam, cohesive zone and FRP sheets, whilst smaller mesh sizes were adopted for the steel plates, bolts and concrete regions surrounding the bolts. Due to severe convergence problems typically associated with strongly nonlinear response and with materials exhibiting non-monotonic stress–strain response [13], such as concrete and cohesive elements, the explicit dynamics solver ABAQUS/EXPLICIT was employed to perform the nonlinear analyses. Quasi-static response was achieved by specifying a slow displacement rate and checking that the kinetic energy was smaller than 2% of the internal energy for the greatest part of the analysis.

4 RESULTS AND DISCUSSION

The F.E. numerical predictions regarding the ultimate shear capacity ($^{num}V_{max}$) and failure modes with the ones observed during testing (see Table 1) are summarized in Table 4.

The ratio of numerically predicted over measured ultimate shear capacity is listed in column 3 of Table 4 with values very close to 1.0, which signifies a very good agreement of the numerically predicted ultimate shear capacity values with the respective experimental ones included in Table 1.
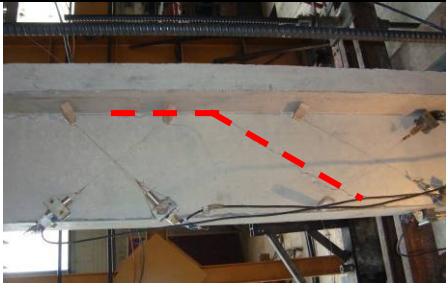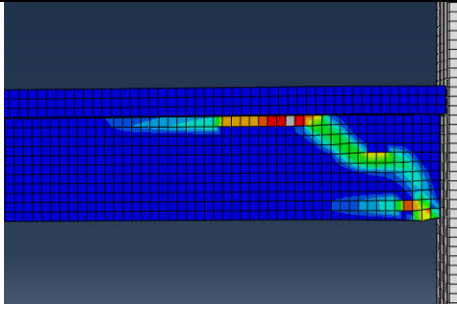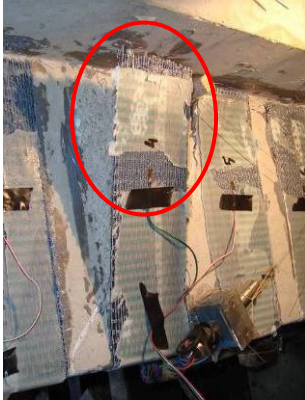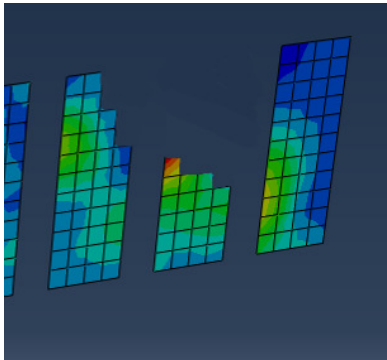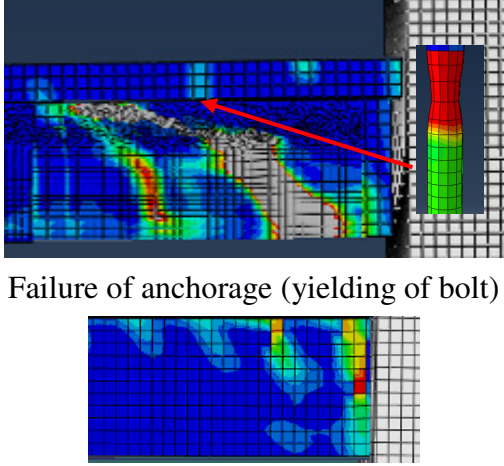
Table 4. Summary of Numerical results and comparison with experimental values.

Designation	Numerical ultimate shear capacity $^{num}V_{max}$ (kN)	$^{num}V_{max}$ / $^{exp}V_{max}$	Numerical failure mode	Experimental failure mode
CTB	37.43	1.00	Diagonal crack	Diagonal crack
TB150	63.63	0.87	Debonding	Debonding
TB150a	187.43	1.03	Anchorage failure	Anchorage failure

Moreover, the numerically predicted modes of failure are also in very good agreement with the ones observed during testing. Detailed discussion for each of the three T-beams considered in the present study follows.

4.1 CTB specimen (non-strengthened)

The observed behavior of the control T-beam specimen, which was tested to obtain the basic structural response of the reinforced concrete beam specimen without the added complexity of the attached SFRP sheets, was, in general, well-predicted by the FE numerical models, as can be seen in Table 5 (1st line), where the experimental and numerical modes of failure are depicted. The experimental failure mode, in the form of the dominant shear crack, and the numerical failure mode of specimen CTB are compared. It should be noted that in all these figures depicting numerical failure modes, the maximum principal plastic strain of concrete is depicted as a means to visualize concrete cracking since no discrete cracks form during the adopted numerical analysis.

Specimen	Experimental failure mode	Numerical failure mode
CTB	 Shear crack	 Shear crack
TB150	 SFRP debonding	 SFRP debonding
TB150a	 Failure of novel anchorage	 Failure of anchorage (yielding of bolt) Some flexural cracks

4.2 TB150 (strengthened with SFRP without anchorage)

The debonding occurred within a thin resin rich layer of concrete, the properties of which were assumed to be incorporated in the cohesive zone material properties. The crack pattern at ultimate load is shown in Table 5 (2nd line). The numerical failure mode is compared with the corresponding experimental one for specimen TB150; as can be seen, an excellent agreement between the experimental and the numerical results is achieved. The beam specimen behaved elastically prior to the formation of the initial flexural cracks, whereupon the flexural rein-forcement prevented the opening of the cracks. Subsequently, a diagonal crack started to form beneath the point of application of the load, which was interrupted by the presence of the FRP

sheets, which were stressed and prevented the opening of the diagonal crack. Finally, the debonding of the FRP sheets commenced and propagated rapidly, leading to the formation of critical diagonal cracks and thus to failure. This observed behavior was also accurately reproduced by the previously described numerical simulations.

4.3   TB150a (strengthened with SFRP with novel anchorage)

As described in section 4.2 the SFRP-strengthened specimen to which no additional anchorage was provided failed abruptly, due to debonding of the SFRP strips. The provision of additional anchorage by means of the device shown in figures 3a and 3b allows for additional forces to be carried by the SFRPs once debonding has occurred; these forces are transferred by the anchoring device finally through the bolts into the concrete thus resulting in an increased ultimate shear capacity and thus in a more efficient utilization of the FRP material. The anchorage zone is stressed from the onset of loading but deformations and stresses remain small as long as the resin remains effective. Upon debonding, the anchorage zone experiences high localized stresses. The failure is no longer due to FRP debonding but rather localized above the anchorage zone, due to the high stresses transmitted by the bolts in the vicinity of the bolt holes. The failure mode is complex and involves a combination of local concrete cracking and yielding of the anchor bolts. The generated complex FE models was in general able to capture the aforementioned failure mode. Table 5 (3rd line) depicts the experimental and numerical failure modes for TB150a with a very good agreement.

5   CONCLUSIONS

- The successful numerical simulation of the application of a novel anchoring device together with open hoop SFRP strips, which enhances the efficiency of these FRP sheets applied as shear reinforcement for reinforced concrete T-section beams, was demonstrated by this study.

- The validation of the numerical simulation is based on the measured behavior of a full-scale reinforced concrete T-beams without nominal shear reinforcement as well as with two (2) full-scale reinforced concrete T-beams that employed open hoop SFRP strips, with or without a novel anchoring device, as a means of upgrading their shear capacity. □

- The success of the deployed numerical simulation is fully demonstrated by comparing first the observed and numerically predicted ultimate shear capacity for all three specimens. The achieved accuracy of the predicted ultimate shear capacity is very good. □

- The success of the deployed numerical simulation is fully demonstrated by then comparing the observed and numerically predicted mode of failure for each one of the three (3) tested specimens. It is shown that the deployed numerical simulations have been articulated with all the significant features, to be able to portray in a very realistic manner complex non-linear mechanisms such as the cracking and crushing of concrete, the debonding and fracture of the SFRP strips and the yielding and fracture of the steel parts of the novel anchoring device. □

- From the above, it must be seen that the accurate numerical prediction of a relatively complex behavior is the result of all these intelligent features that were built into the numerical model together with the accurate representation of all the individual material fea-

tures, which were established by careful testing prior to the numerical simulation. The successful FE models, accurately capturing the basic structural response in terms of ultimate load and failure modes, have been developed and discussed.

- Based on the validated FE numerical models presented here, further research is underway to identify the key features affecting overall structural response and thus to optimize the structural arrangement of the proposed novel anchoring device in terms of strength and ductility.

- A further goal is to derive a generic strengthening technique and associated design guidelines, which allow for a more efficient utilization of the FRPs' strength and significantly enhance the structural performance of existing structures, strengthened with FRP sheets for both static and seismic type loads.

6   ACKNOWLEDGEMENTS

REFERENCES

[1] ACI. Committee 318. Building code requirements for structural concrete and commentary (ACI 318-99). Detroit (MI): American Concrete Institute; 1999.

[2] ACI. Guide for the design and construction of externally bonded FRP systems for strengthening concrete structures (ACI 440.2R-08). In: ACI 440.2R-08. American Concrete Institute: Farmington Hills; 2008. p. 45.

[3] Bakis et al. Fiber-reinforced polymer composites for construction – state of the art review. J Compos Constr 2002 (May). □

[4] Casadei P, Nanni A, Alkhrdaji T, Thomas J. Performance of double-T prestressed concrete beams strengthened with steel reinforcement polymer. Adv Struct Eng 2005;8(4):41.

[5] Chen JF, Teng JG. Shear capacity of fiber-reinforced polymer-strengthened reinforced concrete beams: fiber reinforced polymer rupture. J Struct Eng 2003;129(5):615–25 [May 1, ASCE, 5].

[6] Harper PW, Hallett SR. Cohesive zone length in numerical simulations of composite delamination. Eng Fract Mech 2008;75(16):4774–92.

[7] Hashin Z. Failure criteria for unidirectional fiber composites. J Appl Mech 1980;47(2):329–34.

[8] Hashin Z. Analysis of composite materials – a survey. J Appl Mech, Trans ASME 1983;50(3):481–505. □

[9] Hibbitt, Karlsson, Sorensen. Inc. ABAQUS user's manual volumes I–V and ABAQUS CAE manual. Version 6.10.1. Pawtucket, USA; 2010. □

[10] Kalfat R, Al-Mahaidi R. Investigation into bond of a new CFRP anchorage system for concrete utilizing mechanically strengthened substrate. Compos Struct 2010;92(11):2738–46.

[11] Katakalos K, Papakonstantinou CG, Manos GC. Comparison between carbon and steel fiber reinforced polymer with or without anchorage. In: 6th CICE, Rome; 2012. □

[12] Lu XZ, Teng JG, Yea LP, Jiang JJ. Bond–slip models for FRP sheets/plates bonded to concrete. Eng Struct 2005;27:920–37. □

[13] Manos GC, Katakalos K, Kourtides V. Construction structure with strengthening device and method. European Patent Office, Patent Number WO2011073696 (A1); 2011 (23.06.11). □

[14] Manos GC, Katakalos K, Papakonstantinou CG. Enhanced repair and strengthening of reinforced concrete (R/C) T-beams utilizing external reinforcement of fiber polymer sheets and novel anchoring devices. 15WCEE, Lisboa; 2012. □

[15] Manos GC, Katakalos K, Koidis G, Papakonstantinou CG. Shear strengthening of R/C beams with FRP strips and novel anchoring. J Civ Eng Res 2012;2(6):73–83. http://dx.doi.org/10.5923/j.jce.20120206.04. □

[16] Manos GC, Katakalos K, Kourtides V. Cyclic behaviour of a hybrid anchoring device enhancing the flexural capacity and ductility of an R/C bridge-type pier strengthened with CFRP sheets. J Civ Eng Res 2012. □

[17] Manos GC, Katakalos K. The use of fiber reinforced plastic for the repair and strenghtening of existing reinforced concrete structural elements damaged by earthquakes. In: Masuelli Martin Alberto, editor. Published in the book, Fiber Reinforced Polymers – The Technology Applied for Concrete Repair; January 23, 2013, ISBN: 978-953-51-0938-9 [ch.3]

[18] Manos GC, Katakalos K, Papakonstantinou CG. Shear behavior of rectangular beams strengthened with either carbon or steel fiber reinforced polymers, Applied Mechanics and Materials, 2011

[19] EPPO. Hellenic earthquake planning and protection organization. Athens: Guidelines for Retrofitting in Reinforced Concrete Buildings; 2011.

[20] Papakonstantinou CG, Katakalos K, Manos GC. Reinforced concrete T-beams strengthened in shear with steel fiber reinforced polymers. In: 6th CICE, Rome; 2012.

[21] Papakonstantinou CG, Katakalos K. Flexural behavior of reinforced concrete beams strengthened with a hybrid inorganic matrix-Steel fiber retrofit system, Structural Engineering and Mechanics, 2009

[22] Paz, Mario. International handbook of earthquake engineering: codes, programs and examples. In: Greece by G.C. Manos, editor. Chapman and Hall; 1994. [chapter 17].

[23] Saenz LP. Discussion of ''equation for the Stress–strain curve for concrete'' by Desayi P, Krishnan S. ACI J 1964;61:1229–35.

[24] Smith ST, Teng JG. FRP-strengthened RC beams. I: Review of debonding strength models. Eng Struct 2002;24(4):385–95.

[25] Täljsten B. Defining anchor lengths of steel and CFRP plates bonded to concrete. Int J Adhes Adhes 1997;17(4):319–27.

[26] Täljsten B, Elfgren L. Strengthening concrete beams for shear using CFRP materials: evaluation of different application methods. Compos Part B: Eng 2003;31(2):87–96.

[27] Teng JG, Smith ST, Yao J, Chen JF. Intermediate crack-induced debonding in RC beams and slabs. Constr Build Mater 2003;17(6–7):447–62.

[28] Turon A, Dávila CG, Camanho PP, Costa J. An engineering solution for mesh size effects in the simulation of delamination using cohesive zone models. Eng Fract Mech 2007;74(10):1665–82.

[29] Wu Y, Zhou Z, Yang Q, Chen W. On shear bond strength of FRP-concrete structures. Eng Struct 2010;32:897–905.

[30] Zsutty TC. Beam shear strength prediction by analysis of existing data''. ACI J 1968;65(11):943–51.